Fuel 330 (2022) 125560

Contents lists available at ScienceDirect

Fuel

journal homepage: www.elsevier.com/locate/fuel

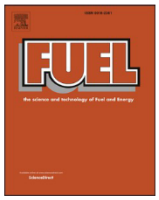

Full Length Article

Ethanol blending effects on auto-ignition and reaction wave propagation under engine-relevant conditions

Jiaying Pan, Yi Ding, Ruoyue Tang, Lei Wang, Haiqiao Wei *, Gequn Shu

State Key Laboratory of Engines, Tianjin University, Tianjin 300072, China

ARTICLE INFO

Keywords:
Gasoline-ethanol blends
Auto-ignition development mode
Low-temperature reaction
Detonation development
Auto-ignition progress

ABSTRACT

Ethanol as an attractive oxygenated fuel is often blended with gasoline to yield beneficial anti-knocking performance. Due to the distinctions in fuel chemistry, the combustion behavior of gasoline-ethanol blends is not fully understood. This study investigated ethanol blending effects on auto-ignition and reaction wave propagation under engine-relevant conditions covering the negative temperature coefficient (NTC) region. Three ethanol blending levels (i.e., E10, E20, and E30 on a volume basis) were introduced into gasoline surrogates. Characteristic timescale analysis for homogeneous auto-ignition was conducted, and localized hotspot auto-ignition and reaction wave propagation was investigated for different gasoline-ethanol blends. Meanwhile, ethanol blending effects on detonation development were comparatively explored. The results show that ethanol addition significantly suppresses fuel reactivity for homogeneous scenarios, especially in low-temperature regions, manifesting prolonged timescales and diminishing NTC behavior. Despite this, different reaction wave propagation modes can be identified during transient auto-ignition and reaction wave propagation, including deflagration, detonation development, and thermal explosion. The detonation wave is always at an underdeveloped status under engine-relevant conditions, and the induced pressure characteristics are sensitive to initial temperatures, hotspot sizes, and fuel reactivity. Meanwhile, ethanol addition tends to promote transient detonation development by elevating the reaction front propagation speed inside the hotspot and enhancing the deflagration to detonation transition outside the hotspot. Such observations are not contrary to that ethanol yields beneficial anti-knocking performance because only chemical effects of ethanol blending are addressed, without considering vaporization cooling effects. The present work demonstrates that ethanol addition globally suppresses engine knocking, but it may induce stronger knocking intensity once end-gas auto-ignition and detonation development are initiated. The current study provides useful insights into ethanol perturbative effects on auto-ignition and reaction wave propagation from chemical perspectives.

1. Introduction

With the reinforcement of fuel economy and emission regulations, downsizing and supercharging technologies have become state-of-the-art in modern spark-ignition (SI) engines. However, downsized SI engines often suffer from heavy knocking and super-knock (also known as low-speed pre-ignition) at high-load operating conditions [1]. The former limits the increase of compression ratio to improve thermal efficiency because of end-gas auto-ignition while the latter limits the desired boost to improve power density owing to developing detonation [2,3]. The knocking mechanism currently remains poorly understood, motivating persistent fundamental investigations.

Controlling knocking processes requires understanding how auto-ignition is triggered but also how it develops. Livengood and Wu [4] investigated the correlations of auto-ignition phenomena in different kinds of apparatus and proposed an integral method to predict end-gas auto-ignition. In the pioneering work, Zel'dovich [5] found different auto-ignition development modes in the mixture with non-uniform reactivity, including subsonic reaction wave propagation, detonation development, and supersonic reaction wave propagation. Lee *et al.* [6] found that a shock wave could be amplified only if the time sequence of heat release was in phase with the shock front itself. Bradley and co-workers [8] expanded upon Zel'dovich gradient theory and proposed an operational detonation diagram consisting of dimensionless parameters. Later, Liberman *et al.* [7] found that detonation development was determined by the steepness of the reactivity gradient and the ratio of

* Corresponding author.
E-mail address: whq@tju.edu.cn (H. Wei).

https://doi.org/10.1016/j.fuel.2022.125560
Received 30 May 2022; Received in revised form 18 July 2022; Accepted 5 August 2022
Available online 22 August 2022

reaction wave propagation speed to characteristic velocities of the issues. Chen and coworkers [9] further extended the detonation diagram into the negative temperature coefficient (NTC) region of large hydrocarbon fuels, and they found that NTC chemistry did not significantly affect auto-ignition development modes. The above studies suggest that the knocking phenomenon in engines is closely associated with auto-ignition development modes. Since then, the detonation diagram has been extensively adopted as a "priori" criterion for predicting engine knock [10,11].

Auto-ignition development modes are significantly affected by various influencing factors, including thermodynamic conditions, chemical reactivity, and turbulent transport. Pan *et al.* [12] found that intense auto-ignition events involving detonation development preferred to occur around the Top Dead Center where thermodynamic conditions and chemical reactivity were higher. Meanwhile, the significant role of pressure wave disturbance in auto-ignition development modes and mode transitions was identified [13]. Chen and co-workers [14] found that detonation development became difficult at higher initial temperatures and detonation regimes for DME and *n*-heptane were not strictly the same. Later, Pan *et al.* [15] investigated the sensitivity of detonation diagrams to fuel property and found that quantitative differences existed in the distribution of detonation regimes between different fuels. Turbulent transport can also affect knocking/detonation transition and thereby knocking intensity. Zhang *et al.* [16] found that a larger turbulent length scale of turbulent Reynolds number reduced knocking strength via mixing enhancement in preheated zones. Luong *et al.* [17] found that decreasing temperature fluctuations and its most energetic length scale mitigated detonation development. Nonetheless, recent experiments showed that fuel reactivity played the first-order significance in strong knocking and detonation development [18]. The above studies have fundamentally highlighted the role of different key parameters in auto-ignition development modes.

It is worth noting that most previous studies mainly address the auto-ignition behavior of a single fuel (e.g., hydrogen, *n*-heptane, and isooctane). However, realistic gasoline fuel contains complex chemical components and is often blended with some oxygenated fuel (e.g., ethanol), which may significantly affect the entire ignition and combustion evolutions [19]. By using Ethanol-Toluene Reference Fuels (ETRF), Netzer *et al.* found [20,21] that the characteristics of auto-ignite in the engine simulations were very different, even though the surrogates possessed the same research octane number (RON). Westbrook *et al.* [22] found that Primary Reference Fuels (PRF) blended synergistically with ethanol while toluene blended antagonistically, and some blends of isooctane and ethanol even exceeded that of neat ethanol. Franken *et al.* [23] found that auto-ignition propensity of Ethanol-Primary Reference Fuels (EPRF) was inhibited with the water addition through physical and chemical effects. Cheng *et al.* [24] found that ethanol addition suppressed low-temperature heat release by the dominance of H-atom abstraction from ethanol. Fan *et al.* [25] found that Ethanol-Toluene-PRF was liable to auto-ignition compared with Ethanol-PRF and Toluene-PRF at low-to-intermediate temperatures, but this tendency became weakened by the enhanced reactivity of ethanol at higher temperatures. The above studies indicate that the auto-ignition behavior of gasoline-ethanol blends has not been fully understood. Furthermore, using ethanol reference fuels for knocking studies, Cho *et al.* [26] found that only fuel-lean spot initiated knocking events due to its higher specific heat ratio and less charge cooling effect. Figueroa-Labastida *et al.* [27] observed that pre-ignition became more likely at the high ethanol concentration while pre-ignition energy release was more pronounced at low temperatures. Different from our general awareness, these investigations demonstrate the complex effects of ethanol addition on auto-ignition and knocking characteristics. However, to the best of the authors' knowledge, there is little literature on the role of ethanol blending effect in auto-ignition development modes during engine knock [28].

With the above considerations, the objectives of the current study are to investigate ethanol blending effects on auto-ignition and reaction wave propagation under engine-relevant conditions. Three ethanol blending levels (i.e., E10, E20, and E30 on a volume basis) were introduced into the Primary Reference Fuel as gasoline surrogates, and high-pressure low-temperature operating conditions (below, within, and above the NTC region) were considered. Characteristic timescale and chemical sensitivity analysis were performed for homogeneous auto-ignition, and hotspot auto-ignition and reaction wave propagation induced by temperature inhomogeneity were investigated via direct numerical simulations. Without endless work on complex geometry configuration, the research issues can well be clarified with little ambiguities in analysis. This study can provide useful insights into the perturbative effect of ethanol on auto-ignition characteristics of standard gasoline and highlight the significance of fuel reactivity in reaction wave propagation.

2. Numerical model and methodology

2.1. Numerical model and methodology

In the simulations, auto-ignition and reaction wave propagation was induced by a hotspot with temperature inhomogeneity in an adiabatic, spherical, constant-volume combustion chamber, as shown in Fig. 1. The initial temperature distribution in the domain is given by:

$$T(t=0,r)=\begin{cases} T_0+(r_0-r)\bullet|\nabla T| & 0\le r\le r_0 \\ T_0 & r\ge r_0 \end{cases} \quad (1)$$

where t and r are the temporal and spatial coordinates, respectively; r_0 is the hotspot radius; ∇T is the temperature gradient within the hotspot; T_0 is the initial temperature outside the hotspot; P_0 is the initial pressure; U_0 is the initial velocity; Y_k is the mass fraction of k th species. The combustion chamber was initially filled with static stoichiometric fuel/air mixtures. An asymmetry boundary condition was employed on the left side and a reflecting wall was defined on the right side. For both boundaries, zero flow velocity and zero concentration stratification were enforced. As the turbulence timescale is around three orders of magnitude larger than the ignition delay time, the absence of turbulence for the auto-ignition study is not unduly restrictive [29]. With this assumption, the current work is focused on the laminar combustion regime.

As aforementioned, a rightward propagating reaction front will be induced in the end-gas mixture with non-uniform temperatures distributions after auto-ignition occurrence. According to Zel'dovich gradient theory [5], there is a critical temperature gradient, $\nabla T_c = (dT/dr)_c$, when the reaction front propagation speed is equal to the local sound speed, a:

$$(dT/dr)_c = ((d\tau_{ig}/dT)\bullet a)^{-1} \quad (2)$$

where T is the hotspot temperature, r is the spatial coordinates, and τ_{ig} is the auto-ignition delay time.

The present work is based on the numerical methodology developed

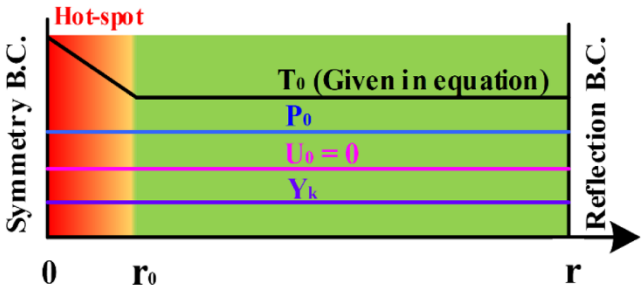

Fig. 1. Schematic of auto-ignition initiation and reaction wave propagation in the combustion chamber.

by Bradley and coworkers [8]. It allows the identification of different auto-ignition development modes according to the characteristics of a single hotspot and the surrounding mixtures. Characteristics of the surrounding mixtures are directly known or derived from experiments while hotspot properties and their radius have to be estimated. The characterization of these features leads to the definition of the non-dimensional parameter ξ. ξ is a normalized temperature gradient that describes the coupling between the acoustic wave and the propagation of the reaction front:

$$\xi = \frac{a}{u_a} = \frac{a}{(dr/dT)(dT/d\tau_{ig})} \tag{3}$$

where u_a is the reaction wave propagation speed.

Theoretically, the particular case of detonation results from the ideal coupling of the acoustic wave and the propagation of the reaction front (i.e., $a = u_a$). However, a developing detonation is not stringently restricted to the critical value $\xi = 1$ due to species and thermal diffusion. Depending on the reactivity, a wider range of initial conditions can lead to a developing detonation, which can be categorized by an upper and lower limit. It is worth noting that as an average status within the hotspot, the reference initial temperature at $r = r_0/2$ is often used to determine τ_{ig} and τ_e and then used to calculate ξ. Within a narrow range of initial temperature variations, the impact of reference location on non-dimensional parameters can be neglected.

Transient auto-ignition initiation and reaction wave propagation was simulated using an in-house code A-SURF. In A-SURF, the second-order-accurate Strang splitting fractional-step procedure is utilized to separate the time evolution of the stiff reaction term from that of the convection and diffusion terms. In the first fractional step, the non-reactive flow is solved. The Runge-Kutta, central difference, and MUSCL-Hancock schemes, all of the second-order accuracy, are employed for the calculation of the temporal integration, diffusive flux, and convective flux, respectively. The chemistry is solved in the second fractional step by using the VODE solver and the Well-Stirred-Reactor (WSR) model is applied in each cell for reactive flow solution. The ASURF has been successfully used in studies about flame propagation, hot-spot auto-ignition, and detonation development [30,31]. The details on the governing equations, numerical methods, and code validations can be found in Refs. [30–32]. In the simulations, the CFL number was kept constant, and the time step was reduced as the finest mesh size was decreased. The finest mesh size was 1.6 μm and the corresponding time step size reached 0.5 ns.

2.2. Operating conditions for numerical simulations

In this work, auto-ignition development modes were investigated in a domain of $r =$ 4.0 cm, and different hotspot sizes ($r_0 =$ 2.0 and 5.0 mm) were employed. Without complex synergistic effects between ethanol and toluene, three ethanol blending levels (i.e., E10, E20, and E30 on a volume basis) were introduced into the Primary Reference Fuels as gasoline surrogates. The baseline case denoted by E0 refers to the standard gasoline with an octane number of 92. The compositions and fuel properties of gasoline-ethanol blends can be found in Table 1.

It is worth noting that despite the crossed reactions between gasoline surrogate and ethanol [22], it supposes that the fuel property varies monotonously within the current range of ethanol addition. Three initial temperatures (i.e., $T_0 =$ 823 K, 880 K, and 945 K) at a fixed initial pressure of $P_0 =$ 4.0 MPa were employed, which corresponds to the temperature region below, within, and above the NTC regime, respectively. Ignition delay time and mixture reactivity are crucially important for auto-ignition initiation and auto-ignition development modes. Therefore, a skeletal PRF-ethanol chemical mechanism [33] developed from the detailed Lawrence Livermore National Laboratory mechanism [34] was employed, which was tested against a wide range of combustion targets, including ignition delay time and laminar flame speed.

Table 1
Compositions and fuel property of stoichiometric gasoline-ethanol blends.

Item	E0	E10	E20	E30
Ethanol (vol %)	0	10	20	30
n-C7H16 (mol %)	8.93	6.81	5.26	4.06
i-C8H18 (mol %)	91.09	69.51	53.64	41.46
C2H5OH (mol %)	0	23.68	41.11	54.48
RON (-)	92.0	95.0	98.2	100.0
MON (-)	82.0	84.2	85.8	87.0
Lower heat (MJ/mol)	4.51	4.16	3.86	3.61

3. Results and discussion

3.1. Ethanol blending effects on homogeneous auto-ignition

To illustrate the ethanol blending effect on the characteristics of homogeneous auto-ignition, Fig. 2 shows the ignition delay time and critical temperature gradient of different gasoline-ethanol blends. It is observed that with the increase of ethanol in blends, the ignition delay time at millisecond level is globally increased and low-temperature branching reactions are significantly suppressed, manifesting an obvious reduction in fuel reactivity. Meanwhile, critical temperature gradients also seem most sensitive to the NTC behavior, manifesting diminishing non-monotonic variations with ethanol addition until the blending level reaches 20 % in volume. Consequently, different variations in critical temperature gradients are observed as initial temperatures are elevated, i.e. $\nabla T_{c_{T_0=823\ K}} < \nabla T_{c_{T_0=880\ K}} < \nabla T_{c_{T_0=945\ K}}$ for E20 and E30 cases, $\nabla T_{c_{T_0=880\ K}} < \nabla T_{c_{T_0=823\ K}} < \nabla T_{c_{T_0=945\ K}}$ for E10 cases, and $\nabla T_{c_{T_0=945\ K}} < \nabla T_{c_{T_0=880\ K}} \ll \nabla T_{c_{T_0=823\ K}}$ for E0 scenarios. According to auto-ignition gradient theory [8], it is generally accepted that a greater critical temperature gradient means a larger spatial temperature gradient is required to successfully achieve detonation development as there is an interaction between pressure wave and reaction wave when $\xi = a/u_a \approx 1$. Large critical temperature gradients often correspond to high chemical reactivity, which corresponds to high temperatures (or low temperatures below the NTC region) and high fuel reactivity. Caused by ethanol blending effects, the variations in ignition delay time and critical temperature gradients will affect auto-ignition initiation and reaction wave propagation under thermal stratification conditions.

Auto-ignition processes also involve heat release which manifests combustion intensity. Fig. 3 shows the excitation time and characteristic velocity of gasoline-ethanol blends. It is observed that the excitation time τ_e at the microsecond level is decreased with the elevation of initial

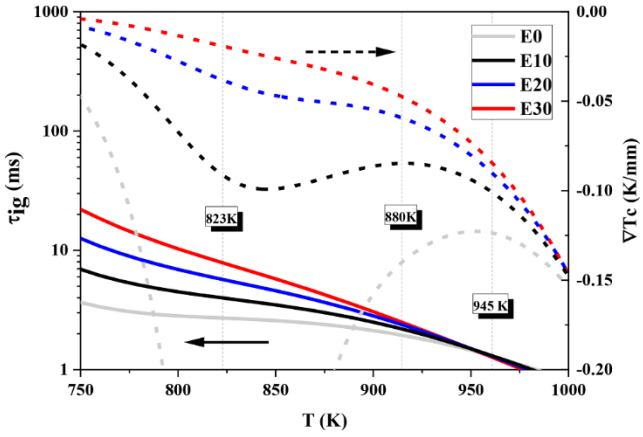

Fig. 2. Ignition delay time and critical temperature gradient of different gasoline-ethanol blends. The ignition delay time is calculated by the adiabatic constant-volume reactor. The critical temperature gradient can be expressed by $\nabla T_C = (dT/d\tau_{ig})/a$.

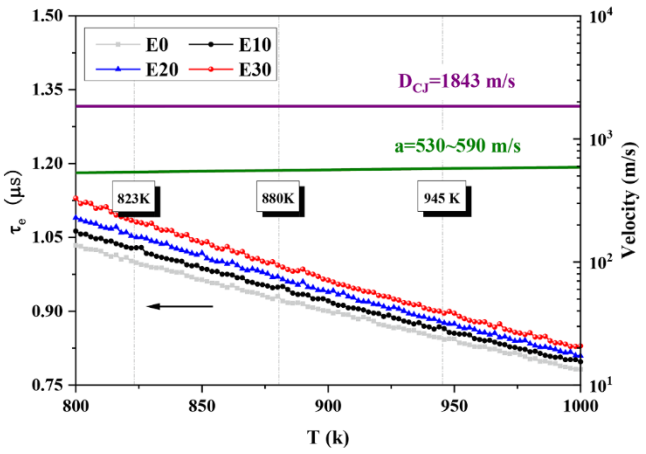

Fig. 3. Excitation time and characteristic velocity of different gasoline-ethanol blends.

temperatures while increasing with ethanol addition, and the initial temperature shows a greater impact on excitation time. The excitation time ranges $\tau_e = 0.78 \sim 1.13\ \mu s$ for the initial temperature of $T_0 =$ 800 1000 K. The prolonged characteristic timescale in heat release caused by ethanol addition also indicates the reduction of reactivity in gasoline-ethanol blends. However, it is noted that different from the ignition delay time exhibiting NTC behavior, the excitation time i s not affected by low-temperature reactions, and it varies monotonically with initial temperatures and ethanol addition. This is because the excitation time is obtained based on the time interval between 5 % and the maximum heat release rate, which mainly allows for high-temperature heat release. Regarding the characteristic velocity, there are almost no variations in the C-J detonation speed (approximate 1843 m/s) and the local sound speed (around 530 ~ 590 m/s) among different gasoline-ethanol blends.

3.2. Ethanol blending effects on reaction wave propagation

Fig. 4 shows the evolutions of temperature and pressure during reaction wave propagation for E0 scenarios. It is seen that for a given hotspot size, different auto-ignition development modes can be observed with the increase of ξ. Specifically, the $\xi = 1.0$ case shown in Fig. 4 (a) corresponds to a supersonic deflagration where a pressure wave follows a preceding reaction wave. The $\xi = 2.0$ case shown in Fig. 4 (b) denotes a developing detonation where the reaction wave catches up and couples with the preceding pressure wave. The $\xi = 4.0$ and 8.0 cases shown in Fig. 4 (c) and (d) represent the subsonic deflagration with and without detonation development, respectively. It is observed that due to the thermal explosion in the end-gas region, detonation development is transient and unsteady, accompanied by obvious variations in peak pressure. Therefore, as ξ is elevated, supersonic deflagration, detonation development, and subsonic deflagration are sequentially observed, with thermal explosion and laminar flame propagation as limit cases.

Knocking intensity in SI engines is closely associated with the evolutions of pressure characteristics during knocking combustion. To illustrate the pressure characteristics of different auto-ignition development modes, Fig. 5 shows the correlations between the ξ and

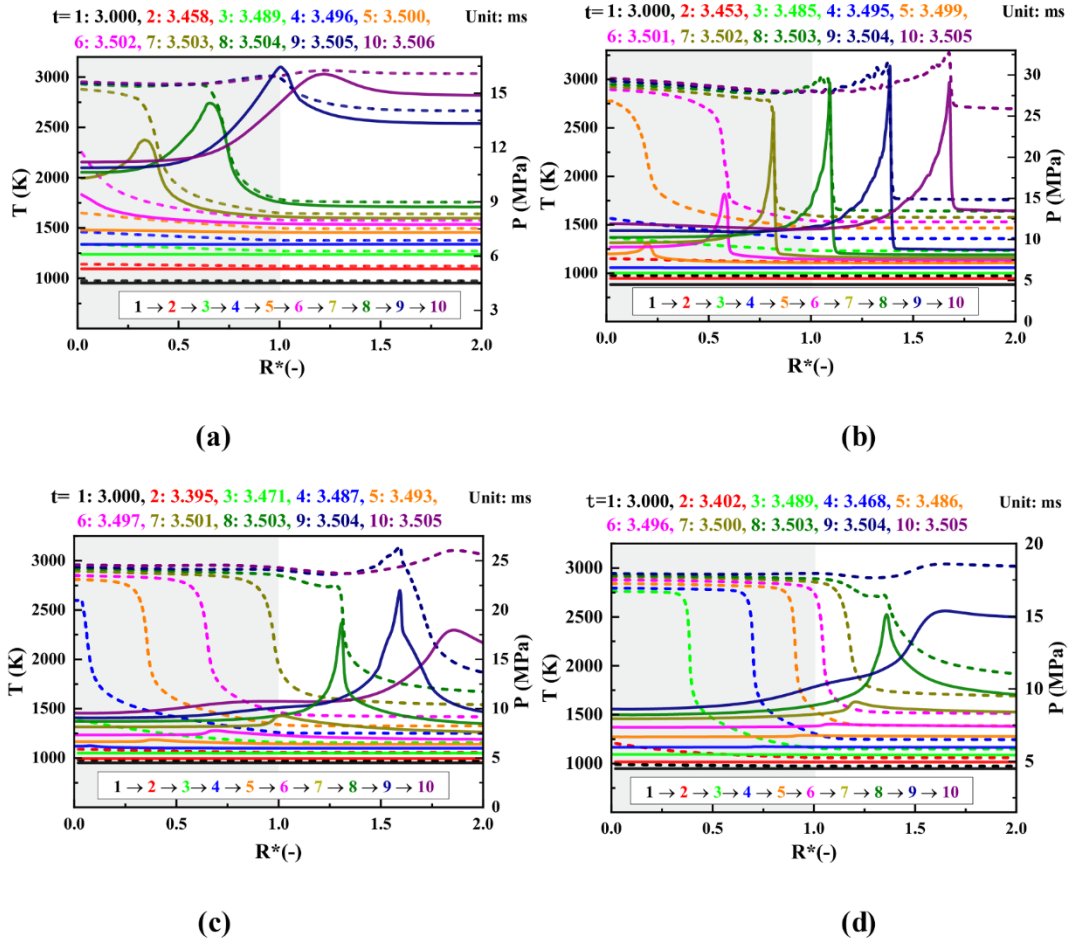

Fig. 4. Evolutions of temperature T (dash line) and pressure P (solid line) for E0 scenarios at $T_0 = 880$ K and $r_0 = 5.0$ mm. (a) $\xi = 1.0$, (b) $\xi = 2.0$, (c) $\xi = 4.0$, and (d) $\xi = 8.0$. R*$= r/r_0$ denotes the normalized hotspot radius and the dark region denotes hotspot interior.

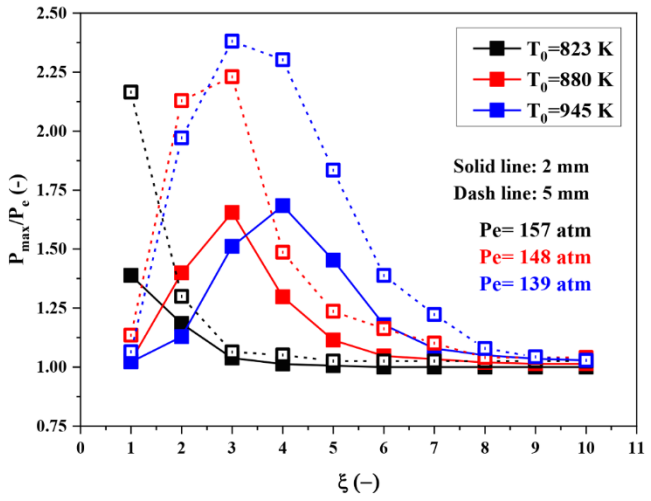

Fig. 5. Correlations between ξ and normalized pressure for E0 scenarios.

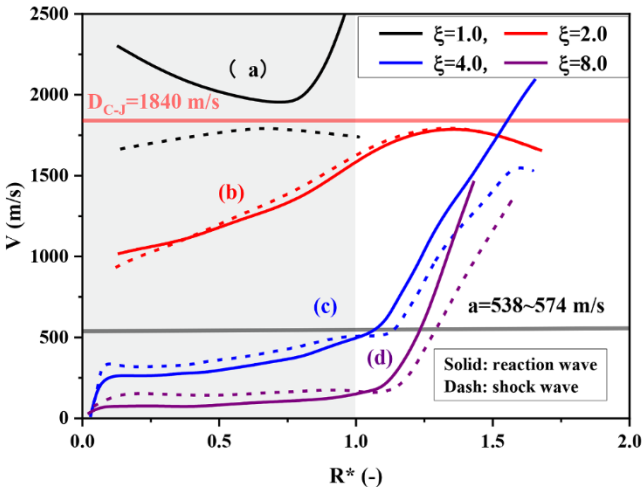

Fig. 6. Propagation speed of auto-ignition reaction wave, detonation speed, and local sound speed for E0 blends at $T_0 = 880$ K with $r_0 = 5.0$ mm. R*= r/r_0 denotes the normalized hotspot radius and the dark region denotes the hotspot interior.

normalized pressure for E0 scenarios. Herein the normalized pressure is defined as the ratio of the maximum pressure to the equilibrium pressure under constant-volume conditions. A larger normalized pressure represents a greater possibility of detonation development and thereby severer knocking intensity. For the current cases at $P_0 =$ 40 atm, the equilibrium pressure is $P_e = 157$, 148, and 139 atm at $T_0 =$ 823, 880, and 945 K, respectively.

It is observed that with the increase of ξ, the normalized pressure is first increased and then decreased at $T_0 = 880$ and 945 K while it is directly reduced to the unit level at $T_0 = 823$ K. Such that the ξ corresponding to the maximum normalized pressure is increased from $\xi \approx 1.0$ to 4.0 as initial temperatures are elevated from $T_0 = 823$ K to 945 K. Such that despite $\nabla T_{c_{T_0=945\ K}} < \nabla T_{c_{T_0=880\ K}} \ll \nabla T_{c_{T_0=823\ K}}$ for E0 scenarios, detonation development tends to occur at smaller ξ. The underlying reasons seem more relevant to low-temperature reactivity instead of faster species and thermal diffusion at higher temperatures (as compared with Figs. 8 and 9). Meanwhile, the amplitude of normalized pressure is globally elevated as the initial temperature is increased. Hotspot size also shows a significant influence on the amplitude of normalized pressures. For $r_0 =$ 2.0 mm cases, the maximum pressure is around one time higher than the equilibrium pressure (i.e., $P_{max}/P_e \approx$ 1.68), whereas it is elevated to two times higher ($P_{max}/P_e \approx 2.38$) at $r_0 =$ 5.0 mm. This is because detonation tends to achieve a fully developed status through deflagration to detonation transition under large-scale thermal stratification conditions. Overall, detonation development and pressure characteristics are significantly affected by both initial temperatures and hotspot sizes.

Fig. 6 further shows the propagation speed of different auto-ignition reaction waves, with the C-J detonation speed and the local sound speed for comparison. It is observed that with the increase of ξ, reaction wave propagation speed decreases significantly within the hotspot interior, across the C-J detonation speed at 1840 m/s and the local sound speed at 538 ~ 574 m/s, and finally approaches the subsonic propagation speed. Specifically, for the case of $\xi = 1.0$ shown in Fig. 6 (a), the auto-ignition reaction wave propagates forward ahead of the shock wave and the corresponding propagation speed is beyond the C-J detonation speed. The cases of $\xi = 2.0$ and 4.0 shown in Fig. 6 (b) and 6 (c) represent the detonation development where there is an inherent coupling between reaction wave and pressure wave within the hotspot interior, through which the propagation speed passes through the local sound speed and approaches the C-J detonation speed outside the hotspot. The $\xi =$ 8.0 case shown in Fig. 6 (d) presents a steady subsonic propagation speed around 80 ~ 160 m/s within the hotspot interior, and then the reaction wave accelerates to a supersonic level. However, the subsequent reaction wave propagation is eventually destroyed by a thermal explosion due to end-gas auto-ignition after a certain residence time.

To illustrate the ethanol blending effect on auto-ignition initiation and reaction wave propagation, Fig. 7 shows the evolutions of pressure and heat release rate during reaction wave propagation of different gasoline-ethanol blends. It is observed that despite the initial prolonged characteristic timescales (e.g., ignition delay time and excitation time), the deflagration to detonation transition is greatly promoted with ethanol addition, manifesting a shorter transition distance and more robust detonation development before end-gas auto-ignition. Specifically, compared with the E0 case shown in Fig. 7 (a) featuring transient detonation development, a deflagration to detonation transition is achieved just outside the hotspot for E10 cases, as shown in Fig. 7(b). Meanwhile, the peak pressure and heat release rate reach 34.0 MPa and 1×10^{15} J/m^{3}s, respectively. Whereas for E20 and E30 cases shown in Fig. 7(c) and (d), the process of deflagration to detonation transition is already finished within the hotspot interior, behaving typical detonation characteristics in reaction wave structure. It is worth noting that despite the promotion of ethanol addition in detonation development, a thermal explosion outside the hotspot can still be observed, similar to the E0 scenarios shown in Fig. 4. Meanwhile, this tendency becomes more obvious with high levels of ethanol addition. This implies that ethanol addition promotes detonation development within the hotspot interior while reducing the chemical reactivity and auto-ignition progress outside the hotspot.

Fig. 8 shows the correlations between ξ and normalized pressure for E30 scenarios. Similar to the E0 scenarios shown in Fig. 5, the significant role of initial temperatures and hotspot sizes in normalized pressures can still be observed. The peak normalized pressure is almost doubled as hotspot size is increased, approaching $P_{max}/P_e \approx 1.75$ and 2.51 at $r_0 =$ 2.0 mm and 5.0 mm, respectively. Meanwhile, the normalized pressure is first increased and then decreased to the unit level with the increase of ξ. However, it is worth noting that the ξ corresponding to the maximum normalized pressure shows a negative correlation with initial temperatures due to the change in ∇T_c, which is just the opposite of the E0 scenarios affected by low-temperature reactions. Specifically, the magnitude of the ∇T_c under different initial temperatures changes a lot with ethanol addition. (i.e. $\nabla T_{c_{T_0=945\ K}} < \nabla T_{c_{T_0=880\ K}} \ll \nabla T_{c_{T_0=823\ K}}$ for E0 cases while $\nabla T_{c_{T_0=823\ K}} < \nabla T_{c_{T_0=880\ K}} < \nabla T_{c_{T_0=945\ K}}$ for E30 cases as shown in Fig. 2). Since $\xi = \nabla T / \nabla T_C$, the variations in the magnitude of ∇T_c under different temperature leads to the change in the above ξ trend. Besides, compared with E0 scenarios, the ξ corresponding to the maximum normalized pressure in Fig. 8 increases significantly at low temperatures

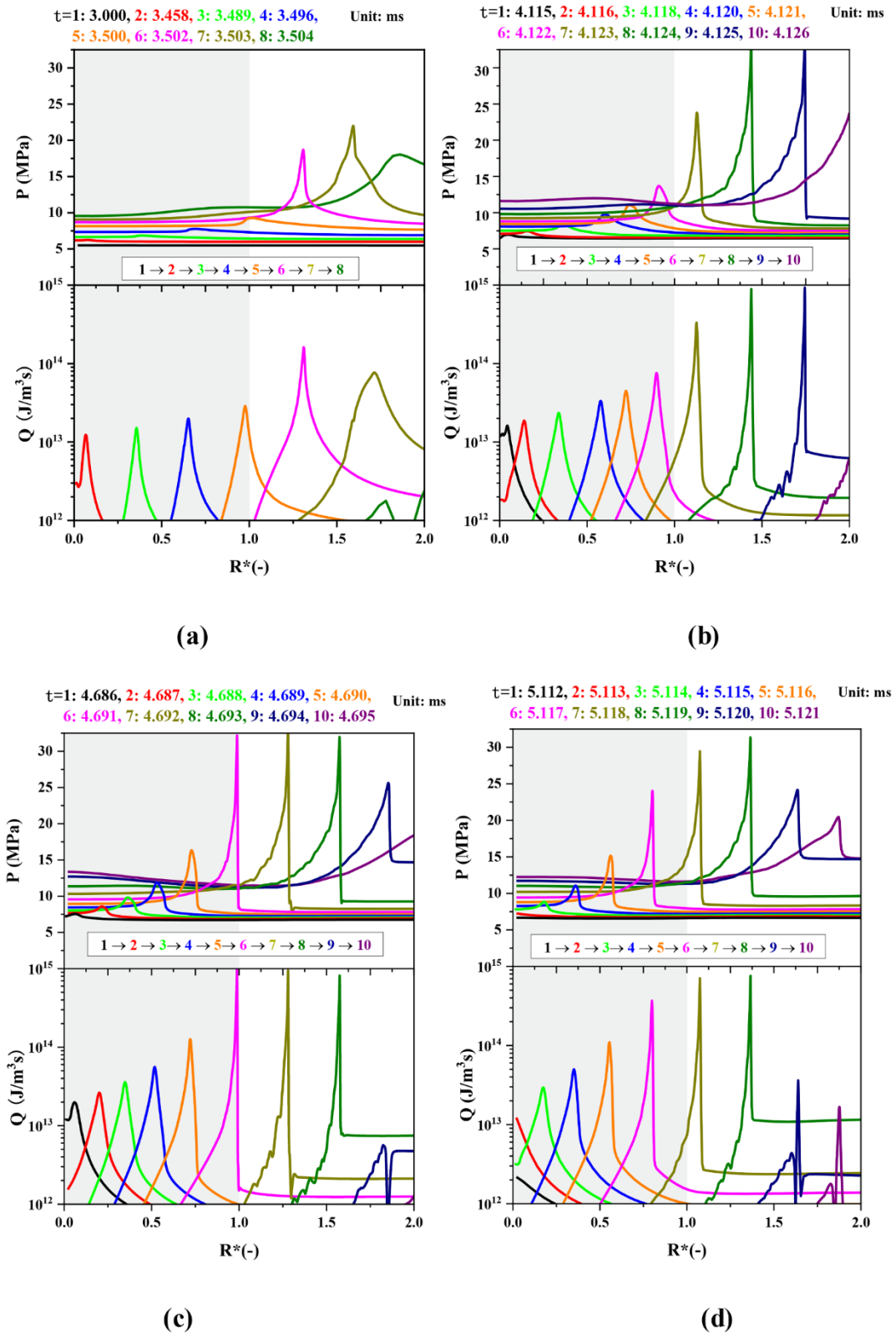

Fig. 7. Evolutions of pressure P and heat release rate Q for different gasoline-ethanol blends at $T_0 = 880$ K, $r_0 = 5.0$ mm, and $\xi = 8.0$. (a) E0, (b) E10, (c) E20, and (d) E30. $R^* = r/r_0$ denotes the normalized hotspot radius and the dark region denotes the hotspot interior.

and does not change greatly at high temperature. This is mainly because the addition of ethanol suppresses the chemical reactivity of the fuel, and this suppression becomes more pronounced at medium and lower temperatures where the role of low-temperature reactions is significant.

To further illustrate the ethanol blending effect, Fig. 9 shows the correlations between ξ and normalized pressure for different gasoline-ethanol blends at $T_0 = 880$ K. It is observed that the maximum amplitude of normalized pressure is not sensitive to ethanol addition (approximate $P_{max}/P_e = 2.25$), and due to $\nabla T_{c_{E30}} < \nabla T_{c_{E20}} < \nabla T_{c_{E10}} < \nabla T_{c_{E0}}$, there is an increase in the ξ corresponding to the maximum normalized

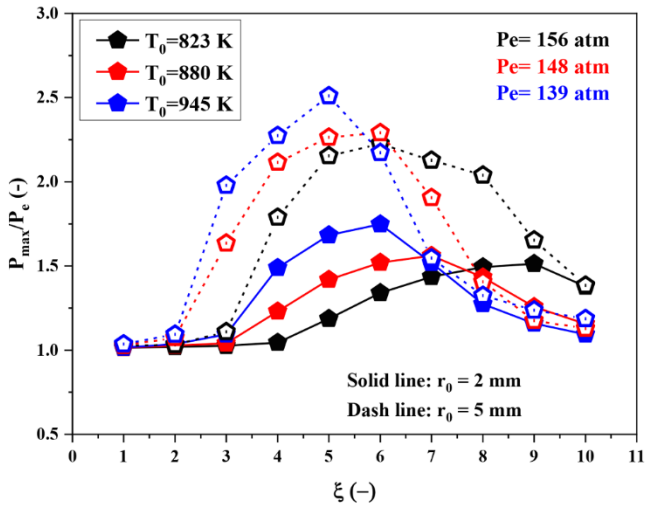

Fig. 8. Correlations between ξ and normalized pressure for E30 scenarios.

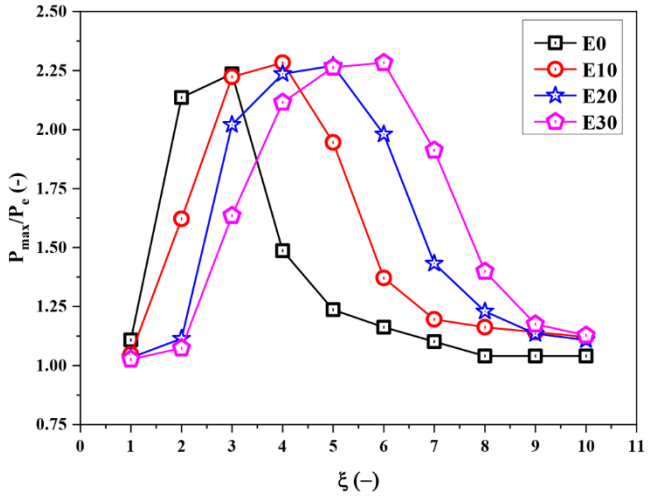

Fig. 9. Correlations between ξ and pressure for E0-E30 scenarios at T_0 = 880 K and r_0 = 5.0 mm.

pressure. Moreover, Fig. 9 also shows that the addition of ethanol expands the ξ range involved in the severe knocking regime. Further combined with the previous analysis, it can be obtained that the addition of ethanol can change the fuel reactivity and its gradient by suppressing the low-temperature reactions, which promotes detonation development under engine-relevant conditions.

Fig. 10 shows the propagation speed of the auto-ignition reaction wave of different gasoline-ethanol blends. It is observed that consistent with the combustion evolutions aforementioned, the reaction wave propagation speed is significantly increased with ethanol addition, especially within the hotspot interior, manifesting the enhanced interactions between reaction wave and pressure wave and the earlier deflagration to detonation transition. It is worth noting that besides E10 scenarios, the reaction wave propagation speed of different gasoline-ethanol blends does not reach C-J detonation speed as the reaction wave propagation is subsequently destroyed by a thermal explosion due to end-gas auto-ignition. Despite this, there are no obvious variations in the peak normalized pressure with ethanol addition, as shown in Fig. 9. This indicates that the detonation development of different gasoline-ethanol blends is at transient and unsteady status under engine-relevant conditions.

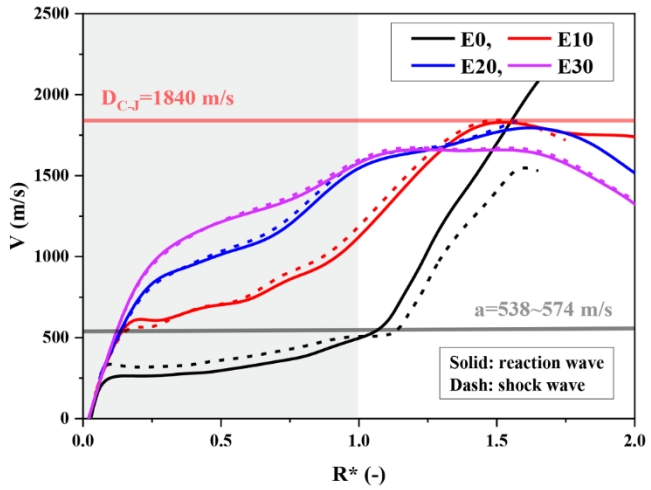

Fig. 10. Propagation speed of auto-ignition reaction wave with detonation speed and sound speed for comparisons. $R^*= r/r_0$ denotes the normalized hotspot radius and the dark region denotes the hotspot interior.

3.3. Ethanol blending effects on detonation development mode

To demonstrate ethanol blending effects on detonation development, Fig. 11 shows the ξ for detonation development at different gasoline-ethanol blends. It is observed that the range of the ξ for detonation development becomes widened with ethanol addition, especially under low levels of ethanol addition. This implies the promotion effect of ethanol addition on detonation development. Meanwhile, such promotion effects can be also observed in r_0 = 5.0 mm case, in which the regime for detonation development becomes larger. This is because detonation development requires enough time for the coupling and mutual reinforcement between chemical reactions and pressure waves. Besides, compared with T_0 = 880 K and 945 K, a larger detonation development regime is observed at T_0 = 823 K, especially at r_0 = 5.0 mm, indicating the enhancement of the detonation development mode.

Theoretically, detonation development involves the competition between the reactivity gradient within the hotspot and the mixture reaction progress outside the hotspot. The former mainly affects auto-ignition modes by influencing reaction front propagation speed, while the latter affects auto-ignition modes by modifying the reaction progress which is critical for deflagration to detonation transition. If end-gas mixture reactivity maintains at a limited level, the reaction front can always develop into a detonation wave before a thermal explosion. To illustrate these correlations, Fig. 12. shows the deflagration to detonation transition distance (DDTD). It can be observed that detonation formation can be located both inside and outside a hotspot. Specifically, the detonation formation inside the hotspot corresponds to smaller ξ and the one outside the hotspot prefers larger ξ. Meanwhile, for a given ethanol addition, the DDTD increases with elevated ξ because larger ξ generally corresponds to lower reaction front propagation speed. For a given ξ, the DDTD significantly decreases with ethanol addition, which is due to the promotion of ethanol addition on reaction front propagation speed.

To clarify how ethanol addition affects rection front propagation, Fig. 13 shows the distribution of ignition delay time gradient and rection front propagation speed just before auto-ignition occurrence. Due to the lower reactivity of ethanol as compared with gasoline, the ignition delay time becomes prolonged with ethanol additions. As such the mixture within the hotspot become more homogeneous due to the thermal diffusion and mass diffusion during a long residence time. Consequently, ethanol addition increases reaction front propagation speed at a reduced reactivity gradient within the hotspot, which results in a shorter DDTD.

It is worth noting that besides the influence on reaction front propagation within the hotspot, the role of ethanol addition is also reflected

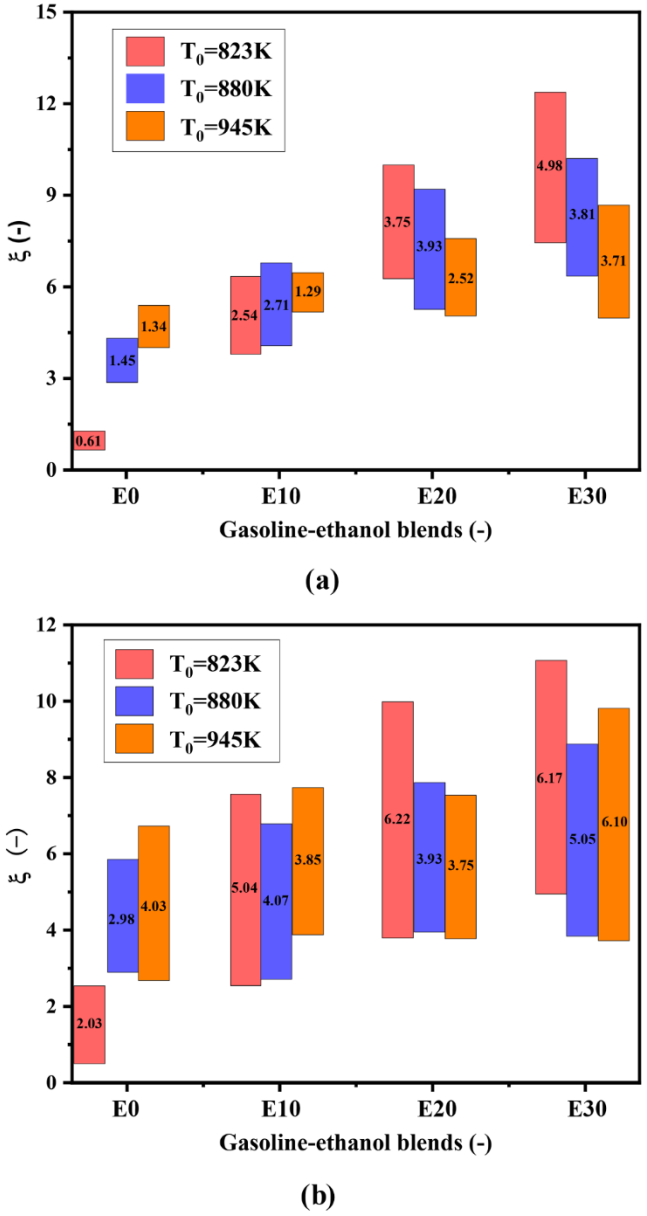

Fig. 11. Normalized temperature gradients for detonation development at different gasoline-ethanol blends. (a) $r_0 = 2.0$ mm and (b) $r_0 = 5.0$ mm. The number on the bar indicates the range of ξ.

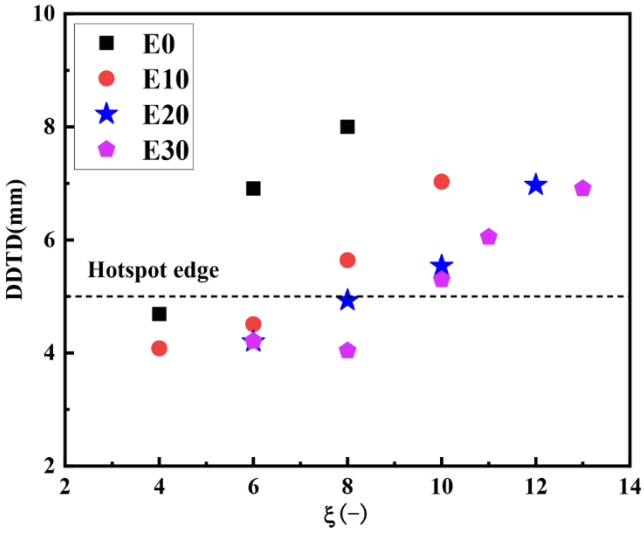

Fig. 12. Deflagration to detonation transition distance (DDTD) for different gasoline-ethanol blends at various ξ with $T_0 = 880$ K and $r_0 = 5.0$ mm.

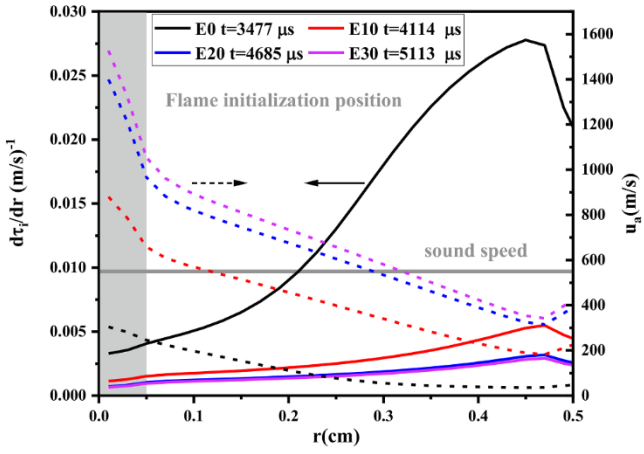

Fig. 13. Distribution of ignition delay time gradient and reaction front propagation speed within the hotspot just before auto-ignition occurrence for different ethanol additions at $T_0 = 880$ K, $r_0 = 5$ mm, and $\xi = 8$.

in the deflagration to detonation transition outside the hotspot. Fig. 14 summarises the correlations between fuel oxidation and auto-ignition modes based on the above numerical results. Herein a diagram consisting of the remaining fuel fraction and ξ is plotted to demarcate detonation development and thermal explosion modes. For the remaining fuel fraction, $Z = Y_t/Y_0$, Y_t is the transient fuel mass fraction and Y_0 is the initial fuel mass fraction. A large remaining fuel fraction corresponds to weak chemical reaction progress. It is observed that the significance of chemical reaction progress in detonation development can be well clarified. Specifically, detonation development prefers to occur in the cases with larger remaining fuel fraction while thermal explosion corresponds to the scenarios with lower remaining fuel fraction. With the increase of ethanol addition, detonation development is shifted to the region with larger remaining fuel fraction, while with the increase of ξ, the thermal explosion manifesting lower remaining fuel fraction is promoted. This implies for given thermal stratifications, ethanol addition can elevate the amplitude of critical chemical reactivity for detonation development, which then promotes the detonation development under engine-relevant conditions. However, this is not contrary to that ethanol yields beneficial anti-knocking properties because only chemical effects of ethanol blending are addressed, and the vaporization cooling influence is not considered here. Recent optical experiments also support these observations, in which ethanol addition globally suppresses engine knocking but it may induce stronger intensity once end-gas auto-ignition and detonation development are initiated [28].

4. Conclusions

In this study, ethanol blending effects on auto-ignition and reaction wave propagation were investigated under engine-relevant conditions covering the negative temperature coefficient (NTC) region. Different levels of ethanol blending were introduced into gasoline surrogates and ethanol blending effects on fuel reactivity were considered. Characteristic timescale analysis for homogeneous auto-ignition was performed, and localized hotspot auto-ignition and reaction wave propagation were investigated.

First, ethanol addition significantly suppresses fuel reactivity of gasoline surrogates, especially in low-temperature regions, manifesting

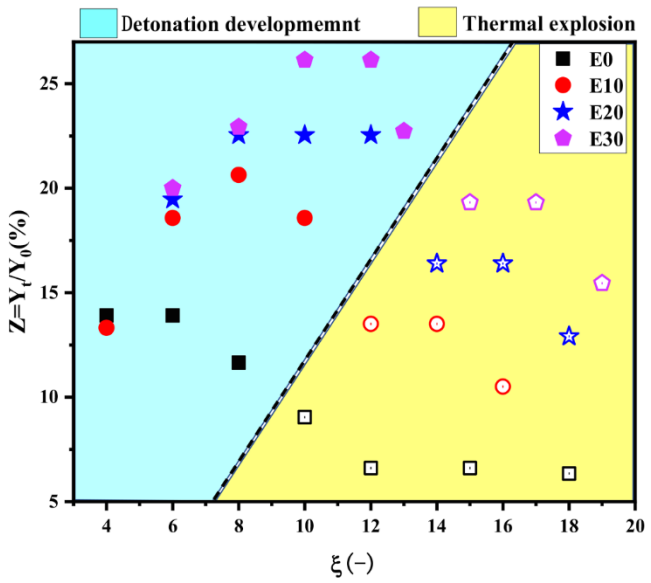

Fig. 14. Diagram of remaining fuel fraction (Z) and ξ for end-gas mixture just before deflagration to detonation transition.

prolonged ignition delay and excitation timing and diminished NTC behavior. Critical temperature gradients seem most sensitive to low-temperature reactions, exhibiting nonmonotonic variations at different initial temperatures, and this observation has vanished when ethanol blending reaches 20 %.

Second, despite inhabited homogeneous auto-ignition with ethanol addition, different reaction wave propagation modes can still be observed, i.e., deflagration, detonation development, and thermal explosion. Meanwhile, the detonation development always proceeds at an underdeveloped status under engine-relevant conditions. Initial temperatures and hotspot sizes positively correlate with the induced pressure amplitude of detonation development, while ethanol addition affects detonation development mainly by modifying ξ. Affected by low-temperature reactions, detonation development prefers lower ξ, which is contrary to the scenarios with ethanol addition.

Finally, both initial temperatures and ethanol addition show significant influence on detonation development modes, manifesting large variations of ξ. Ethanol addition tends to promote transient detonation development through elevating reaction front propagation speed inside hotspot and enhancing deflagration to detonation transition outside the hotspot. This can be observed from the deflagration to detonation transition distance and the fuel remaining fraction as a function of ξ. Such observations are not contrary to the beneficial anti-knocking performance of ethanol addition. It demonstrates ethanol addition globally suppresses knocking, but it may induce stronger intensity once end-gas auto-ignition and detonation development are initiated.

CRediT authorship contribution statement

Jiaying Pan: Conceptualization, Data curation, Formal analysis, Writing – original draft. **Yi Ding:** Writing – review & editing. **Ruoyue Tang:** Data curation. **Lei Wang:** Data curation. **Haiqiao Wei:** Funding acquisition, Project administration, Validation. **Gequn Shu:** Data curation.

Declaration of Competing Interest

The authors declare that they have no known competing financial interests or personal relationships that could have appeared to influence the work reported in this paper.

Data availability

The data that has been used is confidential.

Acknowledgment

This work was supported by the National Key R&D Program of China (2022YFE0100100) and the National Natural Science Foundation of China (52076149, 51825603).

References

[1] Wang Z, Liu H, Reitz RD. Knocking combustion in spark-ignition engines. Prog Energy Combust Sci 2017;61:78–112.
[2] Pan J, Shu G, Wei H. Interaction of flame propagation and pressure waves during knocking combustion in spark-ignition engines. Combust Sci Technol 2014;186:192–209.
[3] Kalghatgi G. Knock onset, knock intensity, superknock and preignition in spark ignition engines. Int J Engine Res 2018;19(1):7–20.
[4] Livengood JC, Wu PC. Correlation of autoignition phenomena in internal combustion engines and rapid compression machines. Proc Combust Inst 1955;5(1):347–56.
[5] Y.B. Zel'dovich. Regime classification of an exothermic reaction with nonuniform initial conditions. Combust Flame 1980;39:211–4.
[6] Lee JH, Moen IO. The mechanism of transition from deflagration to detonation in vapor cloud explosions. Prog Energy Combust Sci 1980;6:359–89.
[7] Liberman MA, Kiverin AD, Ivanov MF. Regimes of chemical reaction waves initiated by nonuniform initial conditions for detailed chemical reaction models. Phys Rev E 2012;85:056312.
[8] Gu XJ, Emerson DR, Bradley D. Modes of reaction front propagation from hot spots. Combust Flame 2003;133(1-2):63–74.
[9] Dai P, Chen Z, Chen S, Ju Y. Numerical experiments on reaction wave propagation in n-heptane/air mixture with temperature gradient. Proc Combust Inst 2015;35:3045–52.
[10] Qi Y, Wang Z, Wang J, He X. Effects of thermodynamic conditions on the end gas combustion mode associated with engine knock. Combust Flame 2015;162(11):4119–28.
[11] Robert A, Richard S, Colin O, Poinsot T. LES study of deflagration to detonation mechanisms in a downsized spark ignition engine. Combust Flame 2015;162(7):2788–807.
[12] Pan J, Chen L, Wei H, Feng D, Deng S, Shu G. On autoignition mode under variable thermodynamic state of internal combustion engines. Int J Engine Res 2020;21(5):856–65.
[13] Pan JY, Wei HQ, Shu GQ, Chen R. Effect of pressure wave disturbance on auto-ignition mode transition and knocking intensity under enclosed conditions. Combust Flame 2017;185:63–74.
[14] Dai P, Qi C, Chen Z. Effects of initial temperature on autoignition and detonation development in dimethyl ether/air mixtures with temperature gradient. Proc Combust Inst 2017;36(3):3643–50.
[15] Pan JY, Dong S, Wei HQ, Li T, Shu GQ, Lei Z. Temperature gradient induced detonation development inside and outside a hotspot for different fuels. Combust Flame 2019;205:269–77.
[16] Zhang TH, Sun WQ, Wang L, Ju YG. Effects of low-temperature chemistry and turbulent transport on knocking formation for stratified dimethyl ether/air mixtures. Combust Flame 2019;200:342–53.
[17] Luong MB, Desai S, Hernández Pérez FE, Sankaran R, Johansson B, Im HG. A statistical analysis of developing knock intensity in a mixture with temperature inhomogeneities. Proc Combust Inst 2021;38(4):5781–9.
[18] Pan J, Hu Z, Wei H, Wang L, He Y, Wang X. Forced turbulence affected auto-ignition and combustion modes under engine-relevant conditions. Appl Energy Combust Sci 2020;1:100015.
[19] Sarathy SM, Kukkadapu G, Mehl M, Javed T, Ahmed A, Naser N, et al. Compositional effects on the ignition of FACE gasolines. Combust Flame 2016;169:171–93.
[20] Netzer C, Seidel L, Ravet F, Mauß F. Impact of the surrogate formulation on 3D CFD engine knock prediction using detailed chemistry. Fuel 2019;254:115678.
[21] Netzer C, Seidel L, Pasternak M, Lehtiniemi H, Perlman C, Ravet F, et al. Three-dimensional computational fluid dynamics engine knock prediction and evaluation based on detailed chemistry and detonation theory. Int J Engine Res 2018;19(1):33–44.
[22] Westbrook CK, Sjöberg M, Cernansky NP. A new chemical kinetic method of determining RON and MON values for single component and multicomponent mixtures of engine fuels. Combust Flame 2018;195:50–62.
[23] Franken T, Seidel L, Matrisciano A, Mauss F, Kulzer AC, Schuerg F. Analysis of the water addition efficiency on knock suppression for different octane ratings, SAE Int. J Adv Curr Prac Mobility 2020;2:2531–52.
[24] Cheng S, Kang D, Fridlyand A, Goldsborough SS, Saggese C, Wagnon S, et al. Autoignition behavior of gasoline/ethanol blends at engine-relevant conditions. Combust Flame 2020;216:369–84.
[25] Fan Q, Wang Z, Qi Y, Liu S, Sun X. Research on ethanol and toluene's synergistic effects on auto-ignition and pressure dependences of flame speed for gasoline surrogates. Combust Flame 2020;222:196–212.

[26] Cho J, Song HH. Understanding the effect of inhomogeneous fuel–air mixing on knocking characteristics of various ethanol reference fuels with RON 100 using rapid compression machine. Proc Combust Inst 2019;37:4911–9.
[27] Figueroa-Labastida M, Badra J, Elbaz AM, Farooqa A. Shock tube studies of ethanol preignition. Combust Flame 2018;198:176–85.
[28] Pan J, Hu Z, Pan Z, Shu G, Wei H, Li T, et al. Auto-ignition and knocking characteristics of gasoline/ethanol blends in confined space with turbulence. Fuel 2021;294:120559.
[29] Bates L, Bradley D. Deflagrative, auto-ignitive, and detonative propagation regimes in engines. Combust Flame 2017;175:118–22.
[30] Chen Z, Burke MP, Ju Y. On the critical flame radius and minimum ignition energy for spherical flame initiation. Proc Combust Inst 2011;33(1):1219–26.
[31] Pan JY, Shu GQ, Zhao P, Wei HQ, Chen Z. Interactions of flame propagation, auto–ignition and pressure wave during knocking combustion. Combust Flame 2016;164:319–28.
[32] Pan J, Wei H, Shu G, Chen Z, Zhao P. The role of low temperature chemistry in combustion mode development under elevated pressures. Combust Flame 2016;174:179–93.
[33] Liu X, Wang H, Zheng Z, Liu J, Reitz RD, Yao M. Development of a combined reduced primary reference fuel-alcohols (methanol/ethanol/propanols/butanols/n-pentanol) mechanism for engine applications. Energy 2016;114:542–58.
[34] Mehl M, Pitz WJ, Westbrook CK, Curran HJ. Kinetic modeling of gasoline surrogate components and mixtures under engine conditions. Proc Combust Inst 2011;33(1):193–200.